Journal of Power Sources 195 (2010) 3261–3265

Contents lists available at ScienceDirect

Journal of Power Sources

journal homepage: www.elsevier.com/locate/jpowsour

Short communication

Electrical conductivity and thermal expansion of neodymium–ytterbium zirconate ceramics

Zhan-Guo Liu, Jia-Hu Ouyang*, Yu Zhou, Xiao-Liang Xia

Institute for Advanced Ceramics, Department of Materials Science, Harbin Institute of Technology, No. 92, West Da-Zhi Street, Harbin 150001, China

ARTICLE INFO

Article history:
Received 4 November 2009
Received in revised form
27 November 2009
Accepted 27 November 2009
Available online 2 December 2009

Keywords:
$(Nd_{1-x}Yb_x)_2Zr_2O_7$
Electrical conductivity
Impedance spectroscopy
Thermal expansion

ABSTRACT

$(Nd_{1-x}Yb_x)_2Zr_2O_7$ $(0 \le x \le 1)$ ceramics were prepared by pressureless-sintering to obtain dense bulk materials. The electrical conductivity of $(Nd_{1-x}Yb_x)_2Zr_2O_7$ was investigated by complex impedance spectroscopy over a frequency range of 20 Hz to 2 MHz from 723 to 1173 K in air. A high-temperature dilatometer was used to analyze thermal expansion coefficient of $(Nd_{1-x}Yb_x)_2Zr_2O_7$ in the temperature range of 373–1523 K. The measured electrical conductivity obeys the Arrhenius relation. The grain conductivity of each composition in $(Nd_{1-x}Yb_x)_2Zr_2O_7$ gradually increases with increasing temperature. A decrease of about one order of magnitude in grain conductivity is found at all temperature levels when the Yb content increases from $x = 0.3$ to $x = 0.5$. The highest electrical conductivity value obtained in this work is 9.32×10^{-3} S cm^{-1} at 1173 K for $(Nd_{0.7}Yb_{0.3})_2Zr_2O_7$ ceramic. $(Nd_{1-x}Yb_x)_2Zr_2O_7$ ceramics are oxide-ion conductors in the oxygen partial pressure range from 1.0×10^{-4} to 1.0 atm at all test temperature levels. Thermal expansion coefficients of $(Nd_{1-x}Yb_x)_2Zr_2O_7$ gradually decrease with increasing ytterbium content at identical temperature levels.

1. Introduction

Complex oxides with $A_2B_2O_7$ composition, where A represents trivalent rare-earth elements and B denotes tetravalent transition metal elements (Ti, Zr, Hf, Mo, Sn, Pb, etc.), exhibit a pyrochlore-type structure or a defect fluorite-type structure [1]. They have a wide variety of attractive physical and chemical properties, such as high melting point, high thermal expansion coefficient, low thermal conductivity, high thermal stability, high radiation stability and high electrical conductivity. These properties make them suitable for extensive applications such as solid electrolytes, thermal barrier coating materials, nuclear waste host materials and high-temperature heating elements [2–6]. Especially, they are potential solid electrolyte materials due to their excellent electrical properties for intermediate-temperature solid oxide fuel cells applications. Lowering the operating temperature of solid oxide fuel cells has attracted great interest worldwide [7–9]. It is well known that electrical conductivity of oxide electrolytes is affected by different factors such as oxygen vacancy concentration, crystal structure, ionic radius of doped elements [10–12]. In recent years, new $A_2B_2O_7$-type complex oxides with various ionic radius ratios of $r(A^{3+})/r(B^{4+})$ have attracted considerable scientific interest [13–17]. For $(Gd_{1-x}Nd_x)_2Zr_2O_7$ $(0 \le x \le 1)$ ceramics, a significant increase in electrical conductivity was obtained by suitable substitution at the Gd site with isovalent rare-earth cations like Nd in $Gd_2Zr_2O_7$ ceramic [13,14]. The electrical conductivity of $(Gd_{1-x}La_x)Zr_2O_7$ $(0 \le x \le 0.4)$ ceramics prepared by mechanical milling was almost La-content independent from 773 to 1023 K [15,16]. $(Gd_{1-x}Sm_x)_2Zr_2O_7$ $(0 \le x \le 1)$ ceramics were synthesized by pressureless-sintering process, and the highest electrical conductivity value was obtained for $(Gd_{0.5}Sm_{0.5})_2Zr_2O_7$ in the temperature range of 623–873 K [17]. In the present work, electrical conductivity and thermal expansion behavior of $(Nd_{1-x}Yb_x)_2Zr_2O_7$ $(0 \le x \le 1)$ ceramics were investigated.

2. Experimental

$(Nd_{1-x}Yb_x)_2Zr_2O_7$ $(0 \le x \le 1.0)$ powders were synthesized by means of the chemical-coprecipitation and calcination method, using zirconium oxychloride (Zibo Huantuo Chemical Co. Ltd., China; Analytical), neodymium oxide and ytterbium oxide powders (Rare-Chem Hi-Tech Co., Ltd., Huizhou, China; purity ≥ 99.99%) as raw materials. Details of the powder preparation process can be found in our previous work [18]. The powder samples were compacted by cold isostatic pressing at 280 MPa for 5 min, and

* Corresponding author at: Institute for Advanced Ceramics, Department of Materials Science, Harbin Institute of Technology, PO Box 433, No. 92, West Da-Zhi Street, Nangang Dist, Harbin 150001, Heilongjiang, China. Tel.: +86 451 86414291; fax: +86 451 86414291.
E-mail address: ouyangjh@hit.edu.cn (J.-H. Ouyang).

0378-7753/$ – see front matter © 2009 Elsevier B.V. All rights reserved.
doi:10.1016/j.jpowsour.2009.11.135

were then pressureless-sintered at 1973 K for 10 h in air. XRD measurements indicate that $Nd_2Zr_2O_7$ and $(Nd_{0.9}Yb_{0.1})_2Zr_2O_7$ exhibit a single phase of pyrochlore-type structure, and $(Nd_{1-x}Yb_x)_2Zr_2O_7$ ($0.5 \le x \le 1.0$) have a single phase of defect fluorite-type structure, and $(Nd_{0.7}Yb_{0.3})_2Zr_2O_7$ shows mixed phases with pyrochlore-type and defect fluorite-type structure [18]. The relative densities of $(Nd_{1-x}Yb_x)_2Zr_2O_7$ ceramics were found to be more than 95.0% using the Archimedes principle, and these values were almost independent of the Yb content.

The impedance (real and imaginary parts) of $(Nd_{1-x}Yb_x)_2Zr_2O_7$ ceramics were measured by AC impedance with four-probe method in the temperature range of 723–1173 K during heating at a temperature interval of 50 K in air. An impedance/gain-phase analyzer (Solatron™ SI 1260, UK) was used for impedance measurements over a frequency range of 20 Hz to 2 MHz, and the amplitude of the input sinuous signal was 20 mV. Platinum paste was painted as electrodes on both surfaces of each pellet and fired at 1223 K in air. Platinum wires were attached on the electrodes for measurements. Cylindrical disc-shaped specimens with a diameter of 8 mm and a thickness of 1 mm were used for impedance measurements. Oxygen partial pressure $p(O_2)$ dependence of impedance of $(Nd_{1-x}Yb_x)_2Zr_2O_7$ ceramics was also measured in the $p(O_2)$ range of 1.0×10^{-4} to 1.0 atm.

The linear thermal expansion behavior of sintered ceramics from 373 to 1523 K was determined with a high-temperature dilatometer (Netzsch DIL 402C, Germany) in an argon gas atmosphere. The dimension of the specimen was approximately 4 mm × 4 mm × 20 mm, and was carefully polished with 1 μm diamond paste before thermal expansion measurement. The data were continuously recorded during heating at a heating rate of 5 K min^{-1}, and they were corrected using the known thermal expansion of a certified standard alumina.

3. Results and discussion

It is convenient to distinguish between the grain and grain boundary effects using the complex impedance plane plot ($-Z''$ *vs* Z'). Typical impedance diagrams of $(Nd_{1-x}Yb_x)_2Zr_2O_7$ ceramics are shown in Fig. 1, which were obtained at 723 K in air. Fig. 1(a) is impedance diagrams of $(Nd_{1-x}Yb_x)_2Zr_2O_7$ ($x = 0$, 0.1, 0.3) ceramics, which are normally composed of high- and low-frequency arcs, respectively. In the ideal case, the frequency response of grain conductivity of electroded polycrystalline electrolytes can be modeled by a resistor–capacitor (RC) pair in parallel. However, in the present case, in place of capacitor a constant phase element (CPE) is required to model the experimental data [19]. Typical equivalent electrical circuits applied to reproduce such impedance diagrams are inset in Fig. 1(a) and (b), respectively. From fitted results, capacitance values found for the high- and low-frequency arcs are 1.96×10^{-10} and 1.46×10^{-7} F cm^{-1} for $Nd_2Zr_2O_7$, which corresponds to the grain and grain boundary contributions, respectively. For $(Nd_{0.9}Yb_{0.1})_2Zr_2O_7$ ceramic, the values of capacitance for grain and grain boundary are 5.48×10^{-11} and 2.56×10^{-7} F cm^{-1}, respectively. However, the capacitance values for grain and grain boundary of $(Nd_{0.7}Yb_{0.3})_2Zr_2O_7$ ceramic are 2.26×10^{-10} and 9.79×10^{-8} F cm^{-1}, respectively. Fig. 1(b) and (c) is impedance diagrams of $(Nd_{1-x}Yb_x)_2Zr_2O_7$ ($0.5 \le x \le 1.0$) ceramics. Only one distinct contribution manifested in the form of semicircular arc is identified. From Fig. 1(b) and (c), the capacitance values of different semicircular arcs are 1.17×10^{-10} F cm^{-1} for $(Nd_{0.5}Yb_{0.5})_2Zr_2O_7$, 7.95×10^{-11} F cm^{-1} for $(Nd_{0.3}Yb_{0.7})_2Zr_2O_7$, 6.76×10^{-11} F cm^{-1} for $(Nd_{0.1}Yb_{0.9})_2Zr_2O_7$ and 4.45×10^{-11} F cm^{-1} for $Yb_2Zr_2O_7$, respectively. These semicircular arcs in Fig. 1(b) and (c) correspond to the grain contributions. The grain resistance value of each composition, R_g, is determined from the intercepts of

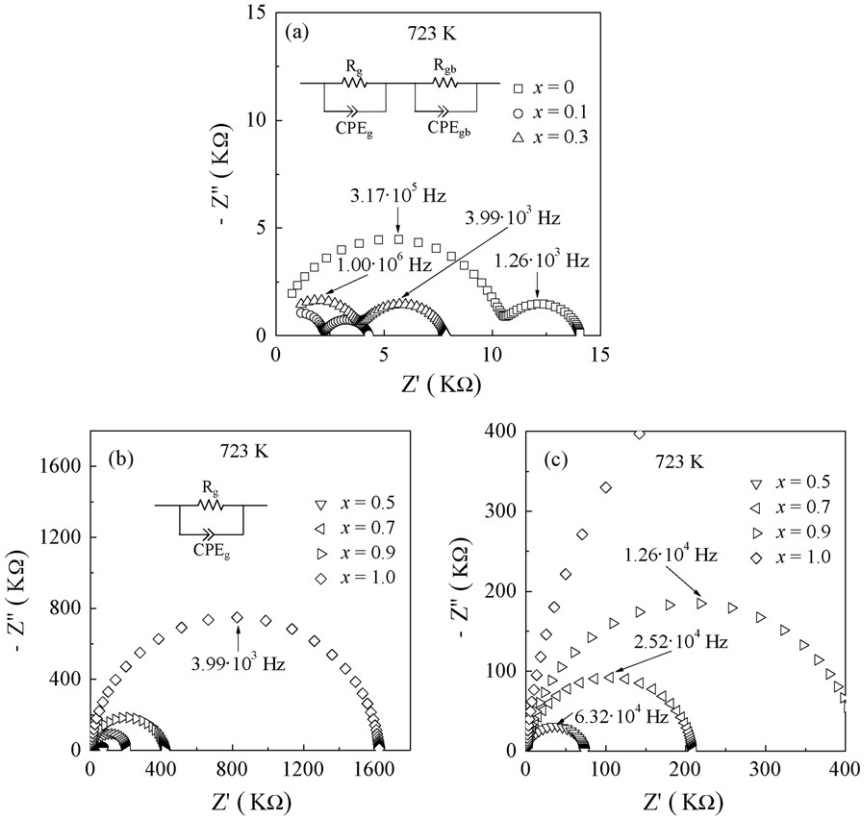

Fig. 1. Typical impedance diagrams at 723 K and schematic equivalent electrical circuits plots (inset) for $(Nd_{1-x}Yb_x)_2Zr_2O_7$ ceramics. (a) $x = 0$, 0.1, 0.3; (b) $x = 0.5$, 0.7, 0.9, 1.0; (c) magnification of (b); R_g, R_{gb}, CPE_g and CPE_{gb} represent grain resistance, grain boundary resistance, constant phase element of the grain and constant phase element of the grain boundary, respectively.

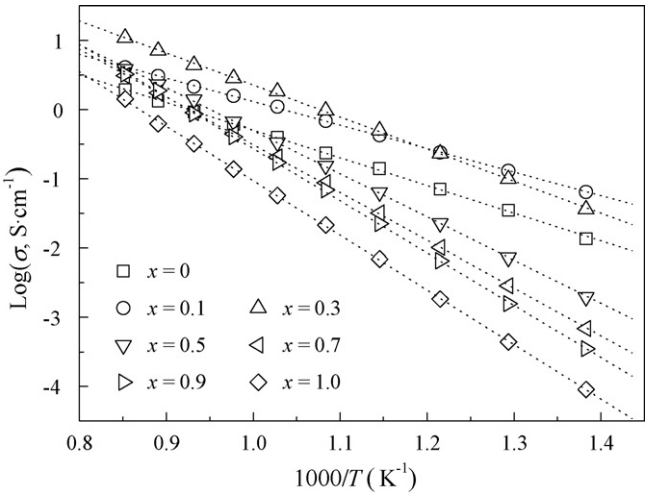

Fig. 2. Arrhenius plots of grain conductivity of $(Nd_{1-x}Yb_x)_2Zr_2O_7$ ceramics.

high-frequency range semicircles on the Z' axes [20]. The grain conductivity of $(Nd_{1-x}Yb_x)_2Zr_2O_7$ ceramics at different temperatures is calculated from the values of resistance and the dimensions of measured specimens.

The temperature dependence of grain conductivity could be plotted based on the Arrhenius equation with the following expression:

$$\sigma_g T = \sigma_{0g} \exp\left(-\frac{E_g}{k_B T}\right) \quad (1)$$

where σ_g, σ_{0g}, E_g, k_B, and T are grain conductivity, pre-exponential factor, activation energy, Boltzman constant, and absolute temperature, respectively. Fig. 2 shows the Arrhenius plots of the grain conductivity for each composition studied in this work, where the lines are fitted to an Arrhenius equation. This confirms that the ionic diffusion process is thermally activated. The activation energy and pre-exponential factor for each composition are calculated from the slope and the intercept of the linear fits in the Arrhenius plots (Fig. 2), respectively. The latter is indicative of the number of charge carriers available for conduction. The calculated values of activation energy and pre-exponential factor are presented in Fig. 3. It is clearly seen that activation energy and pre-exponential factor slightly decrease from $Nd_2Zr_2O_7$ to $(Nd_{0.9}Yb_{0.1})_2Zr_2O_7$ ceramic, and reach a minimum at a ytterbium content of $x = 0.1$, and gradually increase with further increasing ytterbium content. The activation energy of $Nd_2Zr_2O_7$ in this study

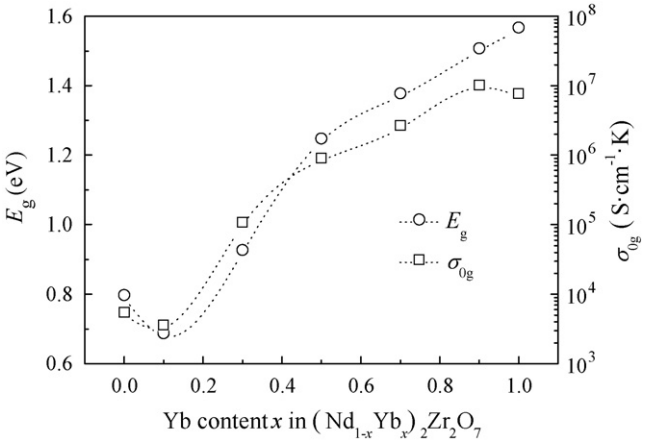

Fig. 3. Activation energy and pre-exponential factor of $(Nd_{1-x}Yb_x)_2Zr_2O_7$ ceramics for grain conductivity as a function of ytterbium content.

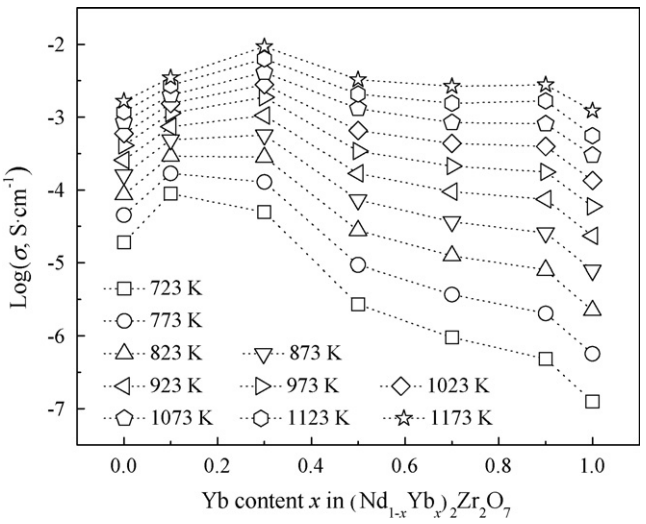

Fig. 4. Variations of grain conductivity of $(Nd_{1-x}Yb_x)_2Zr_2O_7$ ceramics as a function of ytterbium content and temperature.

is 0.79 eV, which is consistent with van Dijk and Burggraff's results [21,22].

Fig. 4 shows the variations of grain conductivity of $(Nd_{1-x}Yb_x)_2Zr_2O_7$ ceramics as a function of ytterbium content and temperature. Clearly, grain conductivity of each composition gradually increases with increasing temperature from 723 to 1173 K. With increasing ytterbium content, the grain conductivity of $(Nd_{1-x}Yb_x)_2Zr_2O_7$ ceramics slightly increases, and then gradually decreases at identical temperature levels. The grain conductivity has a maximum at ytterbium content of $x = 0.1$ or $x = 0.3$ in the temperature range of 723–1173 K. The highest electrical conductivity value obtained in this work is 9.32×10^{-3} S cm^{-1} at 1173 K for $(Nd_{0.7}Yb_{0.3})_2Zr_2O_7$. A decrease of about one order of magnitude in grain conductivity is found at all temperature levels when the Yb content increases from $x = 0.3$ to $x = 0.5$. With further increasing Yb content from $x = 0.5$ to $x = 1.0$, the grain conductivity slightly decreases, and reaches a minimum value at $x = 1.0$ for all temperature levels. The increase in σ_{0g} would lead to an increase in electrical conductivity; however, the increase in E_g would hinder the oxide-ion migration. Thus, these two processes are competing. As the ytterbium content increases from 0 to 0.1, both σ_{0g} and E_g decrease as shown in Fig. 3. From Fig. 4, the electrical conductivity of $(Nd_{1-x}Yb_x)_2Zr_2O_7$ ceramics increases with increasing ytterbium content from 0 to 0.1. This indicates that the decrease in E_g is able to compensate for the decrease in σ_{0g}, and finally causes the increase in electrical conductivity. From Fig. 4, the electrical conductivity of $(Nd_{1-x}Yb_x)_2Zr_2O_7$ $(0.3 \le x \le 0.9)$ gradually decreases with increasing Yb content. This indicates that the increase in σ_{0g} is not able to compensate for the increase in E_g, and finally causes the drop in electrical conductivity. However, the σ_{0g} for $Yb_2Zr_2O_7$ is slightly lower than that of $(Nd_{0.1}Yb_{0.9})_2Zr_2O_7$, while the E_g for $Yb_2Zr_2O_7$ is obviously higher than that of $(Nd_{0.1}Yb_{0.9})_2Zr_2O_7$. Therefore, the electrical conductivity of $Yb_2Zr_2O_7$ is lower than that of $(Nd_{0.1}Yb_{0.9})_2Zr_2O_7$, which is also consistent with the measurement results in this work.

The oxygen partial pressure $p(O_2)$ dependence of electrical conductivity was measured for $(Nd_{1-x}Yb_x)_2Zr_2O_7$ ceramics. Fig. 5 shows the electrical conductivity of $NdYbZr_2O_7$ as a function of oxygen partial pressure $p(O_2)$ at different temperatures. It is clearly seen that electrical conductivity of $NdYbZr_2O_7$ is almost independent of oxygen partial pressure from 1.0×10^{-4} to 1.0 atm at all test temperature levels, which indicates that the conduction is purely oxide-ion conductive with negligible electronic conduction [10].

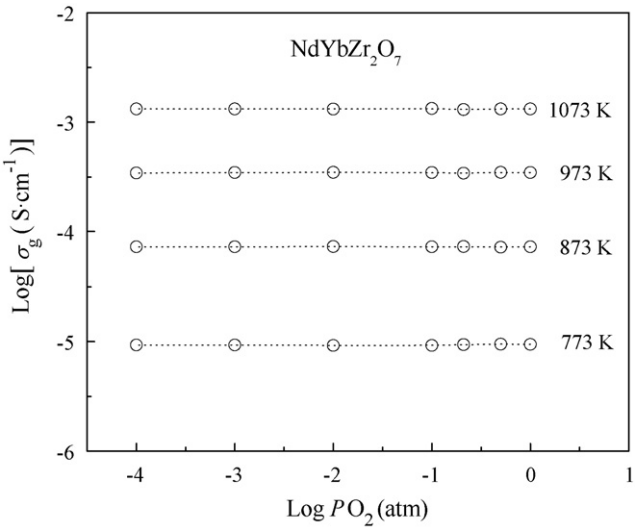

Fig. 5. Oxygen partial pressure dependence of electrical conductivity of $NdYbZr_2O_7$ at different temperatures.

Thermal expansion coefficients of $(Nd_{1-x}Yb_x)_2Zr_2O_7$ ceramics after calibration are shown in Fig. 6. Thermal expansion coefficients of $(Nd_{1-x}Yb_x)_2Zr_2O_7$ ceramics increase rapidly below 500 K, which is caused by the nonlinear increase of instrument temperature, and similar phenomenon was also reported in our previous work [23,24]. Thermal expansion coefficients of $(Nd_{1-x}Yb_x)_2Zr_2O_7$ ceramics increase with the increase of temperature, which is a typical characteristic of solid materials as the atomic spacing increases with the increase of temperature. With increasing ytterbium content, thermal expansion coefficients of $(Nd_{1-x}Yb_x)_2Zr_2O_7$ ceramics gradually decrease at identical temperature levels, and thermal expansion coefficients of $(Nd_{1-x}Yb_x)_2Zr_2O_7$ ceramics at 1523 K are shown in Table 1. Thermal expansion coefficients of $(Nd_{1-x}Yb_x)_2Zr_2O_7$ ceramics at 1523 K are located in the range of $10.62–10.99 \times 10^{-6}\,K^{-1}$.

The results obtained in this work show that $(Nd_{1-x}Yb_x)_2Zr_2O_7$ ceramics are oxide-ion conductors from the low oxygen partial pressure to high oxygen pressure with the highest electrical conductivity of $9.32 \times 10^{-3}\,S\,cm^{-1}$ at 1173 K. Taking into account that electrical conductivity of $(Nd_{1-x}Yb_x)_2Zr_2O_7$ ceramics is slightly lower than that of conventional solid oxide electrolytes, 8 mol.% Y_2O_3 stabilized zirconia (8YSZ), the most likely applications of $(Nd_{1-x}Yb_x)_2Zr_2O_7$ ceramics are in solid oxide fuel cells with thick-

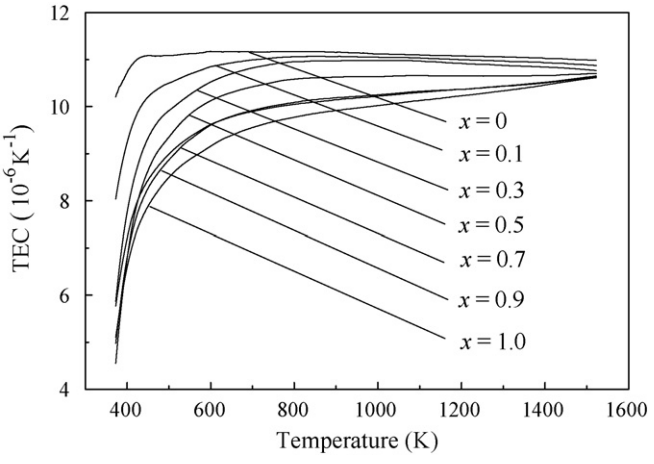

Fig. 6. Thermal expansion coefficients of $(Nd_{1-x}Yb_x)_2Zr_2O_7$ ceramics as a function of temperature.

Table 1
Thermal expansion coefficients of $(Nd_{1-x}Yb_x)_2Zr_2O_7$ ceramics at 1523 K.

Ceramic materials	$\alpha\,(10^{-6}\,K^{-1})$
$Nd_2Zr_2O_7$	10.99
$(Nd_{0.1}Yb_{0.9})_2Zr_2O_7$	10.88
$(Nd_{0.3}Yb_{0.7})_2Zr_2O_7$	10.77
$(Nd_{0.5}Yb_{0.5})_2Zr_2O_7$	10.70
$(Nd_{0.7}Yb_{0.3})_2Zr_2O_7$	10.65
$(Nd_{0.9}Yb_{0.1})_2Zr_2O_7$	10.64
$Yb_2Zr_2O_7$	10.62

film electrolytes, or as protective layers applied onto $LaGaO_3$- or CeO_2-based solid oxide electrolyte materials [25]. At the same time, the moderate thermal expansion coefficients of $(Nd_{1-x}Yb_x)_2Zr_2O_7$ ceramics enable compatibility with these materials [25]. The thermal expansion coefficient of $(Nd_{1-x}Yb_x)_2Zr_2O_7$ ceramics obtained in this work is in the same order of magnitude ($10.0 \times 10^{-6}\,K^{-1}$, 300–1273 K [26]) as that of 8YSZ.

4. Conclusions

The grain conductivity of each composition in $(Nd_{1-x}Yb_x)_2Zr_2O_7$ ceramics gradually increases with increasing temperature from 673 to 1173 K. A decrease of about one order of magnitude in grain conductivity is found at all temperature levels when the Yb content increases from $x = 0.3$ to $x = 0.5$. The grain conductivity has a maximum at ytterbium content of $x = 0.1$ or $x = 0.3$ in the temperature range of 723–1173 K. The highest electrical conductivity value obtained in this work is $9.32 \times 10^{-3}\,S\,cm^{-1}$ at 1173 K for $(Nd_{0.7}Yb_{0.3})_2Zr_2O_7$ ceramic. $(Nd_{1-x}Yb_x)_2Zr_2O_7$ ceramics are oxide-ion conductors in an oxygen partial pressure range of 1.0×10^{-4} to 1.0 atm at all test temperature levels. Thermal expansion coefficients of $(Nd_{1-x}Yb_x)_2Zr_2O_7$ ceramics gradually decrease with increasing ytterbium content at identical temperature levels.

Acknowledgment

The authors would like to thank the financial support from the National Natural Science Foundation of China (NSFC—No. 50972030).

References

[1] M.A. Subramanian, G. Aravamudan, G.V. Subba Rao, Prog. Solid State Chem. 15 (1983) 55–143.
[2] X. Cao, J. Mater. Sci. Technol. 27 (2007) 15–35.
[3] Z.-G. Liu, J.-H. Ouyang, Y. Zhou, J. Li, X.-L. Xia, J. Eur. Ceram. Soc. 29 (2009) 647–652.
[4] B.P. Mandal, A.K. Tyagi, J. Alloys Compd. 437 (2007) 260–263.
[5] K. Shinozaki, M. Miyauchi, K. Kuroda, O. Sakurai, N. Mizutani, M. Kato, J. Am. Ceram. Soc. 62 (1979) 538–539.
[6] P.K. Moon, H.L. Tuller, Solid State Ionics 28–30 (1988) 470–474.
[7] O. Yamamoto, Electrochim. Acta 45 (2000) 2423–2435.
[8] J.W. Fergus, J. Power Sources 162 (2006) 30–40.
[9] S. Hui, J. Roller, S. Yick, X. Zhang, C. Decès-Petit, Y. Xie, R. Maric, D. Ghosh, J. Power Sources 172 (2007) 493–502.
[10] J.B. Goodenough, Annu. Rev. Mater. Res. 33 (2003) 91–128.
[11] S.J. Litzelman, J.L. Hertz, W. Jung, H.L. Tuller, Fuel Cells 8 (2008) 294–302.
[12] D.J.L. Brett, A. Atkinson, N.P. Brandon, S.J. Skinner, Chem. Soc. Rev. 37 (2008) 1568–1578.
[13] B.P. Mandal, S.K. Deshpande, A.K. Tyagi, J. Mater. Res. 23 (2008) 911–916.
[14] B.P. Mandal, A. Dutta, S.K. Deshpande, R.N. Basu, A.K. Tyagi, J. Mater. Res. 24 (2009) 2855–2862.
[15] J.A. Díaz-Guillén, M.R. Díaz-Guillén, J.M. Almanza, A.F. Fuentes, J. Santamaría, C. León, J. Phys.: Condens. Matter 19 (2007) 356212.
[16] J.A. Díaz-Guillén, M.R. Díaz-Guillén, K.P. Padmasree, A.F. Fuentes, J. Santamaría, C. León, Solid State Ionics 179 (2008) 2160–2164.
[17] Z.-G. Liu, J.-H. Ouyang, Y. Zhou, X.-L. Xia, J. Power Sources 185 (2008) 876–880.
[18] Z.-G. Liu, J.-H. Ouyang, Y. Zhou, Q.-C. Meng, X.-L. Xia, Phil. Mag. 89 (2009) 553–564.
[19] J.R. Macdonald, W.B. Johnson, in: E. Barsoukov, J.R. Macdonald (Eds.), Impedance Spectroscopy: Theory, Experiment and Applications, 2nd ed., John Wiley & Sons, Inc., New Jersey, 2005 (Chapter 1).

[20] M.H. Abdullah, A.N. Yussof, J. Mater. Sci. 32 (1997) 5817–5823.
[21] T. van Dijk, K.J. de Vries, A.J. Burggraaf, Phys. Stat. Solidi A 58 (1980) 115–125.
[22] A.J. Burggraaf, T. van Dijk, M.J. Verkerk, Solid State Ionics 5 (1981) 519–522.
[23] Z.-G. Liu, J.-H. Ouyang, Y. Zhou, J. Li, X.-L. Xia, Int. J. Appl. Ceram. Technol. 6 (2009) 485–491.
[24] Z.-G. Liu, J.-H. Ouyang, Y. Zhou, J. Alloys Compd. 472 (2009) 319–324.
[25] V.V. Kharton, F.M.B. Marques, A. Atkinson, Solid State Ionics 174 (2004) 135–149.
[26] M. Mori, T. Abe, H. Itoh, O. Yamomoto, Y. Takeda, T. Kawahara, Solid State Ionics 74 (1994) 157–164.